Highly stable hierarchically structured all-polymeric lubricant-infused films prevent blood stains and repel multi drug-resistant pathogens

Elisabet Afonso[1], Fereshteh Bayat[2], Liane Ladouceur[3], Shadman Khan[2], Aránzazu Martínez-Gómez[1], Jeffrey I. Weitz[2,4,5,6], Zeinab Hosseinidoust[2,7,8], Pilar Tiemblo[1], Nuria García[1], Tohid F. Didar[2,3,8*]

[1] Department of Physical Chemistry of Polymers, Institute of Polymer Science and Technology, Spanish Research Council, Madrid, Spain, 28006

[2] School of Biomedical Engineering, McMaster University, Hamilton, Ontario, L9S 8L7, Canada

[3] Department of Mechanical Engineering, McMaster University, Hamilton, Ontario, Canada L8S 4L8

[4] Department of Medicine, 1280 Main St W, McMaster University, Hamilton, Ontario, Canada, L8S 4L8

[5] Department of Biochemistry and Biomedical Sciences, 1280 Main St W, McMaster University, Hamilton, Ontario, Canada, L8S 4L8

[6] Thrombosis & Atherosclerosis Research Institute (TaARI), 237 Barton Street East, Hamilton, Ontario, Canada, L8L 2X2

[7] Department of Chemical Engineering, McMaster University, Hamilton, Ontario, L9S 8L7, Canada

[8] Michael DeGroote Institute for Infectious Disease Research, McMaster University, Hamilton, Ontario, L98 4L8, Canada

Corresponding author email: didar@mcmaster.ca

ABSTRACT

Thrombus formation and infections caused by bacterial adhesion are the most common causes of failure in blood-contacting medical devices. Reducing interaction of pathogens by using repellent surfaces has proven to be a successful strategy in preventing device failure. However, designing scale-up methodologies to create large scale repellent surfaces remains challenging. To address this need, we have created an all-polymeric lubricant-infused system using an industrially viable swelling-coagulation solvent (S-C) method. This induces hierarchically structured micro/nano features onto the surface, enabling improved lubricant-infusion. Poly(3,3,3-trifluoropropylmethylsiloxane) (PTFS) was used as the lubricant of choice, a previously unexplored omniphobic non-volatile silicone oil. This resulted in all-polymeric liquid-infused

surfaces that are transparent and flexible with long-term stability. Repellent properties have been demonstrated using human whole blood and methicillin-resistant Staphyloccus aureus (MRSA) bacteria matrices, with lubricated surfaces showing 93% reduction in blood stains and 96.7% reduction in bacterial adherence. The developed material has the potential to prevent blood and pathogenic contamination for a range of biomedical devices within healthcare settings.

Keywords: Liquid-infused surfaces, omniphobic lubricant, hierarchicaly structred surfaces, antibacterial, atithrombogenic

INTRODUCTION

Complications related to the surface fouling of medical devices by blood and bacteria remain a major cause of device failure, leading to increased mortality, longer hospitalizations and excessive medical costs. Upon contact with biological fluids such as blood and urine, these synthetic materials are exposed to a cascade of biological entities and physiological responses that commonly result in thrombosis and infection. Specifically, rapid adsorption of plasma proteins onto the surface of blood contacting medical devices initiates a cascade of reactions that ends in clot formation and subsequent thrombosis.[12] In relation to infection, the adherence of bacteria onto the surface of such devices – while initially reversible, often develops into well-established, biofilm-based infections, which are difficult to treat.[3] As a result, surface modification strategies aimed at preventing initial adsorption of blood proteins and microorganisms have garnered significant interest as a means to prohibit device-associated thrombosis and infection. [2,4,5]

A wide range of surface treatment approaches have been developed to improve the blood compatibility and antifouling properties of medical devices. In particular, liquid-infused surfaces (LIS) have been established as an effective strategy to prevent fouling on a wide range of devices, such as grafts, catheters, and implants.[6-11] Since their initial invention,[12] many efforts have been dedicated to the preparation and optimization of different types of LIS systems to maximize lubricant-surface interactions, long term stability, and ease of application.[10,13-19] Many such improvements have focused on minimizing the depletion of the lubricant layer over time, which remains a key hinderance in the real-world applicability of LIS systems.[20-22] To this end, recent studies have determined that having a good lubricant-surface interaction, and a larger surface contact area – achieved by hierarchical structures at the micro and nano scale - successfully delays lubricant depletion off the surface and enhances its stability.[23]

Unfortunately, well-established strategies for the fabrication of hierarchical structures at micro and nano scales – such as lithography, etching, and laser ablation - remain complicated and time-consuming, which poses a challenge for large-scale production. Correspondingly, recent studies have aimed to develop approaches better suited for commercialization.[24] The swelling-coagulation solvent method (S-C) in particular, has garnered significant interest as a simple, fast,

and cheap approach that could be used to manufacture structured polymer surfaces on a large scale. In this method, the micro-nano scale topographies are created *via* simple immersion of the polymer in the swelling solvent, followed by coagulation in a non-solvent solution.[25] This results in the formation of structures in less than an hour.

The use of polymers as substrates for LIS systems is widely expanded due to their inherent flexibility, transparency, and large-scale production potential. Poly (vinilidene fluoride) (PVDF) specifically, has been identified as a suitable substrate for various commercial applications due to its fluorinated chemical nature and its soft processability compared to other fluorinated polymers such as polytetrafluoroethylene (PTFE). The presence of C-F bonds confers high thermal and chemical stability as well as chemical resistance. Paired with the piezoelectricity and pyroelectricity of some of its crystalline phases, PVDF has shown applicability in solar devices, sensors, batteries, molecular separation, conductive polymers and polymer nanocomposites.[26] In medicine, PVDF has been widely exploited[27] for tissue engineering,[28] drug delivery,[29] the fabrication of antibacterial membranes[30] and the manufacturing of biosensors.[31-33] In relation to LIS systems, its fluorinated chemical nature allows for stable interactions with fluorinated lubricants without the need for further modification of surface chemistry.

The miscibility of PVDF with a Polymethyl methacrylate (PMMA) amorphous polymer, has been extensively studied for the crystallinity and morphological characteristics of the different blends.[34,35] Under certain conditions, PMMA favors the β-phase crystallization of PVDF[36,37] and reduces crystallinity. This results in generation of micro/nano structures when exposed to S-C treatments, as the lower crystallinity of the blend leads to increased swelling of the polymer under milder conditions.[25]

Perfluoropolyethers and polydimethylsiloxane oils represent the two classes of lubricants commonly used in LIS systems, due to their low surface tension, low vapour pressure and chemical inertness. On the other hand, fluorinated compounds such as perfluorodecalin (PFD) have typically been used as lubricants in medical applications.[38] The binding of several fluorine atoms to the same carbon atom in compounds such as PFD results in very low London dispersion interactions, which renders the surface both oleophobic and hydrophobic. The main shortfall of these compounds is their high volatility under ambient, open-air conditions. Fluorosilicone oils present a promising alternative, as they are rich in fluorine groups, while also exhibiting low volatility. The use of fluorosilicone oils has previously been reported for various applications both in its cured and oil form,[39] but its integration into LIS systems has not been explored. In particular, poly(3,3,3 - trifluoropropylmethylsiloxane) (PTFS) is a biocompatible fluorosilicone oil that has previously been used for biomedical applications – namely for the treatment of eye diseases such as retinal detachment.[40,41] This lubricant affords high stability when infused onto a substrate due

to its low volatility index, while also being rich in fluorine, thus providing favourable chemical properties and long-term stable LIS for open air conditions.

Herein, we present a LIS system composed of hierarchically micro and nano structured PVDF-PMMA substrates infused with PTFS. The polymer blends were fabricated using melt compounding extrusion and films were prepared using hot pressing – a scalable production process. S-C treatment was used to induce the formation of hierarchical structures, and PTFS was subsequently infused onto the surface to produce PVDF-PMMA LIS. Given the abundance of fluorine groups present on both the substrate and in the lubricant, intermolecular interactions were expected to form between the substrate's surface and lubricant layer, providing an added avenue for stability. We further characterized these surfaces and evaluated their antifouling properties against bacteria and blood.

RESULTS AND DISCUSION

Fabrication of PVDF-PMMA-LIS

In order to create lubricant-infused PVDF-PMMA surfaces, we designed a three-step protocol, as shown in Figure 1. Polymeric surfaces were prepared from a mixture of PVDF and PMMA polymers with a ratio of 80/20% wt. The polymer blend was prepared by a melt compounding extrusion process, followed by hot pressing, which yielded planar surfaces from the extruded blend. The polymeric film was supported on brass in order to prepare thin films, which minimized material waste and limited the introduction of hierarchical structures to only one side of the film (Figure 1a). S-C treatment was performed in two steps: immersion in a hot solvent to induce swelling of the polymer, followed by immersion in a precipitant solvent that acts as a coagulant. The temperature of both solvents and the immersion times were optimized to generate homogeneous surfaces under mild conditions that minimize the cost and time of treatment. Acetone and dimethylformamide (DMF) were both used as swelling solvents, as they induce the formation of surfaces with different topographies (A-S and D-S, respectively). Both swelling treatments were followed by coagulation in ethanol. A-S substrates were formed by acetone-mediated swelling at 54°C, while D-S substrates were prepared *via* DMF-mediated swelling at 70°C (Figure 1b). A-S and D-S were infused with PTFS through a 24h immersion, to obtain A-LIS and D-LIS substrates, respectively (Figure 1c).
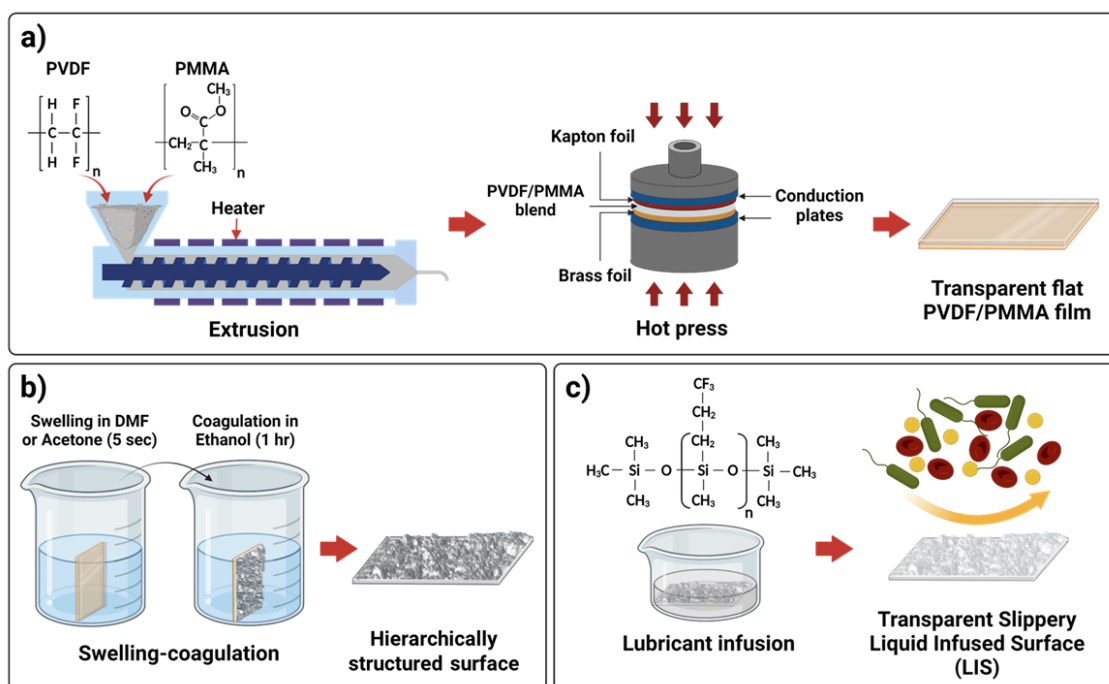
Figure 1. Schematic illustration for the fabrication process. **(a)** Preparation of the polymer blend by melt compounding using an extruder and hot pressing the material to prepare planar films supported by a brass foil. **(b)** S-C treatment by immersion of the supported polymer film in DMF or acetone followed by coagulation in ethanol to prepare the hierarchically structured surfaces (D-S and A-S). **(c)** Infusion of the rough surfaces with lubricant to prepare liquid-infused surfaces (D-LIS and A-LIS).

Characterization of PVDF-PMMA surfaces and LIS.

An exhaustive characterization of the surfaces at all stages (planar, hierarchically structured, and LIS) was carried out. Firstly, the PVDF-PMMA blend was characterized, with PVDF and PMMA neat polymers studied for comparative purposes. All physico-chemical polymer characterization before treatments is found in the Supporting Information. Based on the different degradation temperature of the polymers – 415°C for PVDF *versus* the two-phase degradation of PMMA at 150°C and 250°C, the composition of the blend could be verified by Thermogravimetric Analysis (TGA), shown in Figure S11. In addition, the calorimetric properties of the polymers were studied by Differential Scanning Calorimetry (DSC) shown in Figure S2. A single melting peak was found in the PVDF at 167.5°C. Regarding the PMMA curve, a typical amorphous behavior is obtained without crystallization or fusion peaks. In the PVDF80-PMMA20 blend, a composed endotherm is shown, due to the different crystalline morphology. An endothermic peak at 50°C was also observed, which was previously assigned to the reorganization of the constrained amorphous phase in the proximity of the crystalline phase during heating. Infrared spectroscopy and x-ray diffraction (XDR) were used to identify the different PVDF crystalline phases, shown

in Figure S3 and Figure S4, respectively. Under the processing conditions used in this work, the PVDF neat polymer crystallizes in its α-phase, whereas in the PVDF-PMMA blend, amorphous PMMA prevents α-phase crystallization, rather favoring the β-phase in PVDF. β-phase crystallization in PVDF allows milder conditions to be used in the treatment of swelling and coagulation.[42]

After the characterization of the blend, S-C treatments were carried out to generate hierarchical structures and obtain A-S and D-S from PVDF80-PMMA20 planar films. To verify that the treatment does not lead to the dissolution of either of the two polymers, an XPS test was performed (Figure S5). The D-S sample was evaluated since it received the most aggressive treatment. It was observed that the surface composition after treatment is similar to the initial theoretical composition. After the treatment, the transparent planar film turned white and opaque. This acted as an indication of successful structure generation, since microscale entities induce light scattering, which result in a white-pale color. Hierarchically structured surfaces were then infused with PTFS to obtain A-LIS and D-LIS. Upon infusion, the lubricant immediately spread across the samples and the surfaces regained transparency. This change was induced by the similar refractive indices of the PVDF-PMMA blend[43] and PTFS oil[44] – 1.44 and 1.43, respectively. Transparency indicated that a continuous layer had been formed between the substrate and the lubricant and that all the air gaps present on the surface had been filled. Transparency and flexibility of the material can be seen in Video S1.

The morphology and topography of the micro/nano structured surfaces before and after infiltration process were characterized using Scanning Electron Microscopy (SEM). Figure 2a shows SEM micrographs of A-S, D-S, A-LIS and D-LIS. The top and side view of the surfaces were analyzed. It was observed that different S-C treatments gave rise to different structures, despite the identical chemical nature of the resultant surfaces. A-S surfaces show smaller pores, and the treatment reaches 55 μm deep into the film, measured *via* the side view image. D-S surfaces contained structures that were more open and had larger pores due to the harsher temperature and solvent treatment conditions. In addition, the treatment reaches a greater depth on the film, at approximately 87 μm. In both cases there is nanoscale structuring that can be seen *via* SEM at a magnification of 8000X, where features smaller than 2 μm are visible (Figure 2a.ii and Figure 2a.v). These nanoscale features are instrumental in the interaction of the surface with the lubricant, to prevent its depletion[23]. SEM images obtained after lubricant infusion indicate that PTFS successfully spreads across the surfaces and a smooth layer is formed. In some cases, the inner structure can be seen on the lubricated surfaces, particularly with D-LIS (Figure 2a.x.). Side views of the lubricated samples were also obtained, which demonstrated that PTFS penetrates the porous structures on the hierarchically structured films (Figure 2a.ix and Figure 2a.xii.).

To evaluate the wettability properties of the developed structures we measured the static contact angle and sliding angles of various test liquids as shown in Figure 2b. Wettability with water (surface tension of 72.75 mN/m [45]) was first studied. Planar surfaces had a slightly hydrophilic contact angle of 81.4±1.6°. After S-C treatment, hierarchically structured surfaces A-S and D-S demonstrated superhydrophobic properties, with contact angles greater than 160° and sliding angles less than 10° in the case of D-S, where the drops roll along the surface. When the samples were infused with PTFS, the fluorinated chemical nature of the oil and liquid-liquid interaction between the infused oil and water droplet ensured that the surfaces remained hydrophobic, with contact angles above 95° for both LIS and sliding angles less than 10°.

For the possible application of these surfaces in medical devices, it is important to study the behavior of these surfaces with human whole blood (surface tension of approximately 55 mN/m [46]). In this case, the behavior of the blood on the planar surface is slightly superior to that of the water but lower than the structured surfaces. The main difference was found in the sliding angle, where the blood droplet was pinned to the surface on both hierarchically structured surfaces. Attending to lubricant infused surfaces, repellent behavior was found with contact and sliding angles. A 10 µL-blood droplet was used to reveal the pinning phenomena in D-LIS, marked in the table with * symbol.

To evaluate the oleophobic properties, tests were carried out with hexadecane (surface tension of 27.76 mN/m [47]). On the planar surface, hexadecane demonstrated an oleophilic contact angle of 20°. However, after treatment, hexadecane spread completely over the surfaces on A-S and D-S. After infiltration with the lubricant, hexadecane contact angles of $39.8 \pm 1.7°$ and $41.9 \pm 2.2°$ were demonstrated on A-LIS and D-LIS respectively, showing better performance than planar surfaces. PTFS is immiscible with the hexadecane, causing hexadecane to slide over the surface at low angles. This highlights the difference between planar and LIS surfaces, as both are flat and fluorinated. While the contact angle is similar for water and blood between the two surface types, all liquids pin to the planar surfaces. On LIS both liquids slide at very low angles due to the liquid-liquid interactions between the lubricant layer and the deposited droplet. The sliding behavior of LIS with water and hexadecane can be seen in Video S2 for A-LIS and Video S3 for D-LIS. It was also concluded that there are slight wettability differences between A-LIS and D-LIS. This difference can be attributed to the differences in the lubricant layer once it is infused onto each of these surfaces (see LIS side view on Figure 2a).

To consider the morphological differences between the A-S and D-S surfaces, topography parameters were studied. A table containing the main roughness parameters can be found in Table S1. Although both structures were initially well infused and demonstrated promising sliding angle

properties, structural differences were expected to influence the stability of the lubricant layer in more demanding conditions, dictating their life cycle.
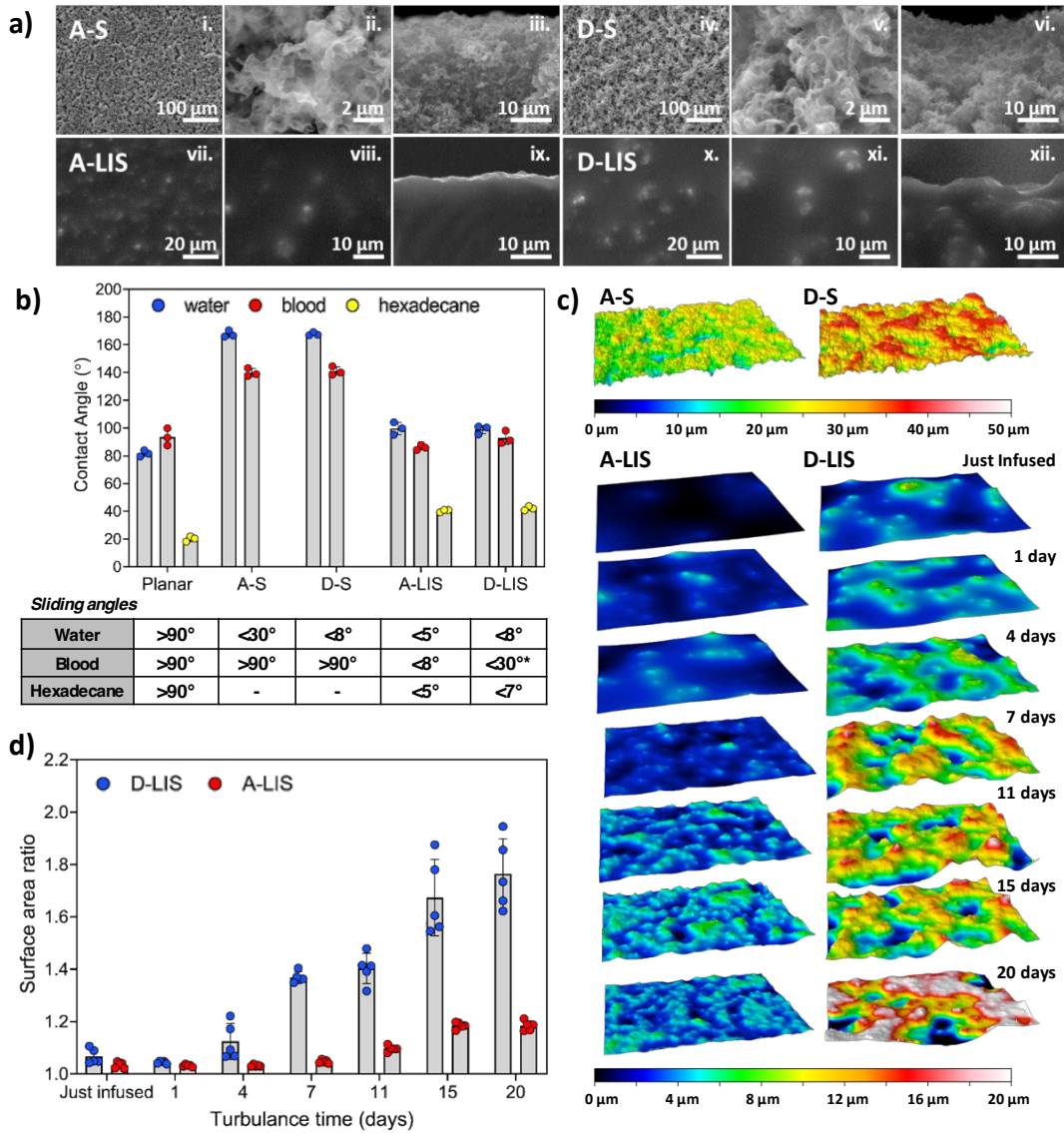

Figure 2. Characterization of surfaces. **(a)** SEM micrographs of the A-S and D-S surfaces before and after infiltration of the lubricant. i, ii. A-S top surface, iii. A-S side surface, iv, v. D-S top surface, vi. D-S side surface, vii, viii. A-LIS top surface, ix. A-LIS side surface, x, xi. D-LIS top surface, xii. D-LIS side surface. **(b)** Wetting properties of planar surfaces, treated surfaces, and lubricant-infused surfaces with water, blood, and hexadecane. The bars represent the contact angles while sliding angles are contained in the table below. 5 µL droplets were used for all measurements and at least 3 replicates were performed **(c)** 3D images obtained by optical profilometry before and after the lubricant infiltration process **(d)** Variation of the surface ratio of the lubricated samples A-LIS and D-LIS over 20 days under turbulent conditions. over the 20-day period. Colored scale bars represent 0-50µm for hierarchically structured surfaces and 0-20µm for lubricated surfaces, respectively.

To assess the impact of morphology on lubricant retention, lubricant stability tests under flow conditions were performed by immersing LIS in water under turbulent flow over a 20-day period. Stability of the lubricant layer was studied using optical profilometry. 3D images of the surfaces were obtained before and after infiltration, and after several immersion trials under turbulence, as shown in Figure 2c. Ratio parameters were obtained at different turbulence times as shown in Figure 2d. It was observed that the D-LIS structure experienced greater lubricant loss, resulting in a considerable increase in surface roughness and ratio. This can be attributed to the differences in topography features and roughness parameters previously mentioned. Despite the chemical and production similarities between the A-LIS and D-LIS, these results highlighted the importance of comprehensive design and characterization of the material, as well as an accurate evaluation of its behavior in the most demanding conditions of use, to simulate real-world applications.

Blood adhesion and antithrombin generation assays

A thrombin generation assay was performed to evaluate the potential use of these substrates as blood-contacting medical devices. As seen in Figure 3a, clotting times with lubricated samples were significantly longer than planar or hierarchically structured films. Whole blood clotting (Figure 3b) and adhesion (Figure 3c) experiments were also performed, to analyze the interactions between blood and the surfaces in their different states (planar, hierarchically structured and lubricated). Results indicated a significantly lower adhesion of the blood to lubricated samples, with no significant difference between A-LIS and D-LIS. Optical images shown above the plots in Figure 3b and Figure 3c were taken immediately following the clotting and absorbance assays and are in line with the obtained results. Surfaces used for the clotting assay were imaged *via* SEM. The excellent performance of A-LIS and D-LIS in blood contacting environments was further demonstrated through SEM images, presented in Figure 3d. Here, it is shown that the planar and treated samples collected significant blood clots on the surface, evidenced through a network of fibrin and red blood cells built up on the surfaces. Conversely, the LIS samples show minimal adhesion of blood to the surface following 1 hour of exposure to recalcified whole blood.
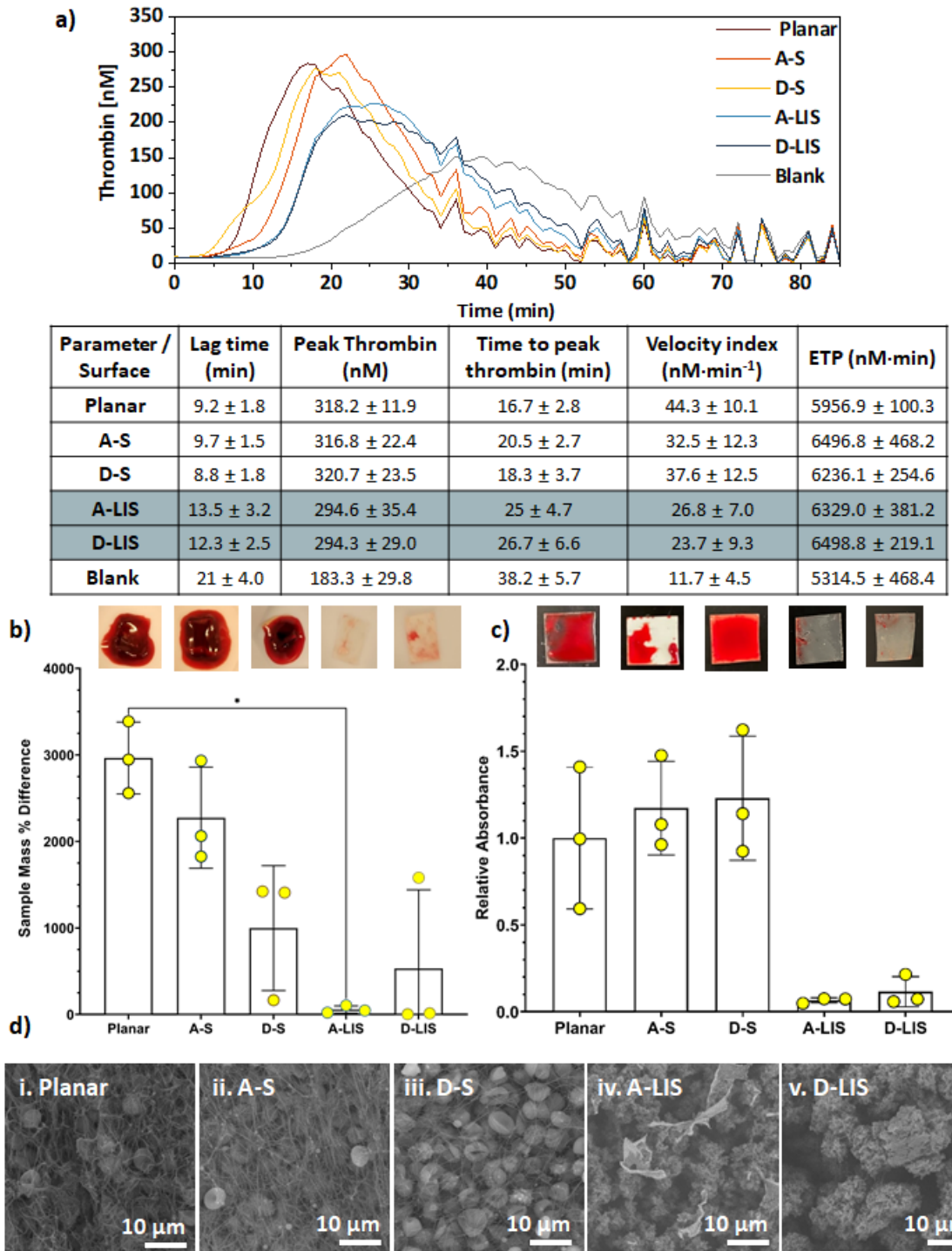
Parameter / Surface	Lag time (min)	Peak Thrombin (nM)	Time to peak thrombin (min)	Velocity index (nM·min^{-1})	ETP (nM·min)
Planar	9.2 ± 1.8	318.2 ± 11.9	16.7 ± 2.8	44.3 ± 10.1	5956.9 ± 100.3
A-S	9.7 ± 1.5	316.8 ± 22.4	20.5 ± 2.7	32.5 ± 12.3	6496.8 ± 468.2
D-S	8.8 ± 1.8	320.7 ± 23.5	18.3 ± 3.7	37.6 ± 12.5	6236.1 ± 254.6
A-LIS	13.5 ± 3.2	294.6 ± 35.4	25 ± 4.7	26.8 ± 7.0	6329.0 ± 381.2
D-LIS	12.3 ± 2.5	294.3 ± 29.0	26.7 ± 6.6	23.7 ± 9.3	6498.8 ± 219.1
Blank	21 ± 4.0	183.3 ± 29.8	38.2 ± 5.7	11.7 ± 4.5	5314.5 ± 468.4

Figure 3. Blood interaction with developed surfaces. **(a)** Representative thrombin vs time is shown. Thrombin generation parameters were measured for blank, planar, treated surfaces A-S and D-S, and lubricant-infused surfaces A-LIS and D-LIS. Values represent means and ±SD of at least 6 samples. **(b)** Relative clot mass adhered to each surface along with representative images of blood clots formed on the surfaces. **(c)** Relative absorbance of the transfer solution measured at 450 nm wavelength along with representative images of blood clots formed on the surfaces. **(d)** SEM micrographs of samples following whole blood clotting assay.

Pathogen adhesion on developed surfaces

To evaluate whether these surfaces were capable of preventing bacterial adhesion following prolonged exposure, bacterial assays were conducted. Among hospital-acquired infections, methicillin-resistant *Staphylococcus aureus* (MRSA) is widely considered a pathogen of concern.[48] MW2, which is a MRSA strain, was used to evaluate the bacterial repellency properties of the surfaces. Bacterial solution was incubated for 24h (Figure 4a.i) and 72h (Figure 4a.ii) with planar, hierarchically structured (A-S and D-S) and lubricated surfaces (A-LIS and D-LIS).
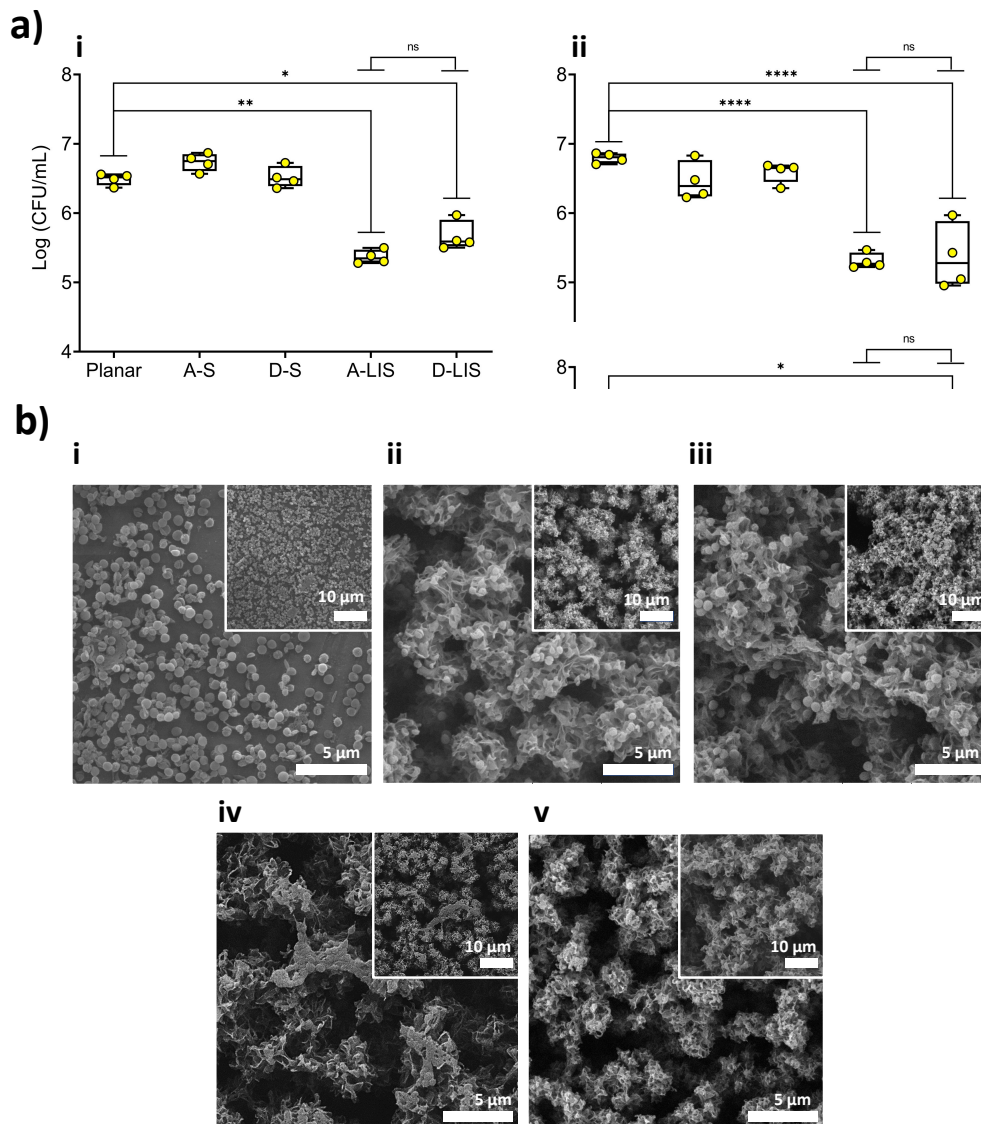

Figure 4. Evaluation of bacterial adhesion on planar, hierarchically structured surfaces D-S and A-S, and lubricated surfaces D-LIS and A-LIS. **(a)** i. MRSA adhesion to surfaces after 24h to surfaces after 72h incubation. Data represent the mean of at least four replicates. Significant reduction was calculated using a one-way ANOVA test and demonstrated across multiple groups indicated here with * (P=0.05); **(P=0.01) and ****(P=0.0001) and ns as no significant

difference. Error bars represent the standard error of the mean. **(b)** SEM micrographs of samples after 72h incubation with MRSA under static conditions. i. Planar, ii. A-S, iii. D-S, iv. A-LIS and v. D-LIS (scale bar 5µm). Inset represents lower magnifications (scale bar 10µm).

For 24h incubation experiments, A-LIS demonstrated 1.1-log reduction corresponding to 92.6% (P<0.01) reduction and D-LIS demonstrated 0.8-log reduction corresponding to 83.64% (P<0.01) reduction in bacterial adhesion relative to planar conditions. No significant differences were demonstrated between lubricated A-LIS and D-LIS surfaces. For 72h experiments, the results indicate a higher reduction, close to 1.5-log. A-LIS and D-LIS surfaces showed a 1.5-log (96.7%) and 1.3-log (94.4%) reduction over the planar surface, respectively.

The samples were imaged after the bacterial assay to evaluate adhesion of MRSA onto the surfaces. These images supported results obtained through the bacterial assay, showing an abundance of MRSA on planar and hierarchically structured A-S and D-S surfaces. However, with the addition of lubricant, a significant decrease in the number of bacteria is observed.

CONCLUSION

We reported a scalable, simple, and fast method for creating a slippery lubricant-infused surface suitable for medical devices. The substrate surface is an all-polymeric material prepared by extrusion and hot-pressing industrial process from its powder form. To generate hierarchical structures a swelling-coagulation treatment based on immersion in solvents was performed. Optimization of the crystallization of the polymer was performed to achieve a structure fabrication treatment using mild conditions of time and temperature. The final treatment is fast, cheap and it can be applied to large surfaces, achieving 10x10 cm surfaces in this work. A detailed study on lubricant stability on different surfaces was performed by using a non-destructive technique, optical profilometry. The fluorinated silicone oil that was used as lubricant is non-volatile, omniphobic and highly stable up on the hierarchically structured substrate surface. Compared to other lubricants used in medical applications, fluorinated silicone is non-volatile and it has omniphobic properties to achieve greater repellency to water, hexadecane, and whole blood. No chemical modification is needed to achieve interaction between lubricant and substrate. This LIS remains flexible and transparent, while demonstrating antifouling properties against blood and bacteria under long-term exposure conditions. Surfaces reported in this work demonstrate 93% reduction in blood stains and 96.7% reduction in multi-drug resistant bacterial adherence. The proposed lubricant-infused material is a promising candidate for applications within clinical care.

MATERIALS AND METHODS

Reagents: Polyvinylidene fluoride (PVDF) in powder form (Kynar 741) was kindly provided by Policomplex S.L. (Valencia, Spain). Polymethyl methacrylate (PMMA) in powder form, Mw

120,000 was purchased from Sigma Aldrich (Darmastadt, Germany). Fluorinated silicon oil, Poly(3,3,3 - trifluoropropylmethylsiloxane) (PTFS) with 80-120 cSt was purchased from Fluorochem (Derbyshire, United Kingdom). Acetone, dimethylformamide (DMF) and ethanol were purchased from Sigma Aldrich, and they have been used without previous purification. Methicillin-resistant S. aureus (MRSA) MW2 strains were kindly provided by Michael Surette. BD Bacto tryptic soy broth, purified agar powder and sodium citrate dihydrate were purchased from Fisher Scientific (Hampton, NH). Yeast extract, D-glucose, and phosphate-buffered saline (PBS) tablets were purchased from VWR (Mississauga, ON, CA). 2-[4-(2-hydroxyethyl)piperazin-1-yl]ethanesulfonic Acid (HEPES) and calcium chloride ($CaCl_2$) were purchased from Bioship Canada (Burlington, ON, Canada). The thrombin-directed fluorescent substrate Z-Gly-Gly-Arg-AMC (ZGGR) was purchased from Bachem (Bubendorf, Switzerland). Pooled plasma citred blood and human whole blood were collected from healthy donors as previously described[49]. Venous blood was collected in tubes containing sodium citrate from healthy volunteers by a licensed phlebotomist. A signed written consent was collected by all donors and all procedures were approved by the McMaster University Research Ethics Board.

Surface preparation: The PVDF80-PMMA20 blend was prepared by melt compounding. First, the powdered polymers were physically mixed in the indicated proportion. The mixture was then melt compounded using a twin-screw Haake Minilab (ThermoFisher Scientific, Massachusetts, USA) extruder operating in extrusion mode at 200°C with screw speed of 80 rpm. Films of the PVDF80-PMMA20 blend were prepared by hot press molding using a P200P press (COLLIN Lab & Pilot Solutions GmbH, Maitenbeth, Germany). For each surface, 2.5 g of the polymer blend was placed between a brass foil that acts as a support and a Kapton foil as a separator that does not adhere to press plates. A 200ºC temperature is applied for 2 minutes to melt the material and then a 150 bar pressure is applied to make the material flow, filling the entire frame. After 5 minutes the film is removed from the press and allowed to solidify at room temperature. Films prepared had 10x10 cm dimensions and 120-130 µm thickness.

Swelling-coagulation treatment: The hierarchically structuredtopography was achieved through a swelling and coagulation (S-C) treatment. Polymer films attached to brass foil were used to achieve the textured layer only on one side and to maintain the dimensionality of the samples during the S-C process as they were relatively thin films. The treatment consisted of immersion in a hot solvent for 5 seconds, acetone at 54 ºC (A) or dimethylformamide at 70 ºC (D), followed by immersion in ethanol for one hour. Two different surface topographies are obtained, namely, A-S and D-S. Finally, the films were left to dry overnight at room temperature. After the treatment, the polymer surfaces were detached from the brass foil by immersion in liquid nitrogen.

Lubricant infusion: The infusion of the lubricant in the hierarchically structured surfaces was achieved by immersion of the surfaces into PTFS oil lubricant for 24 hours. Two cycles of 10-minutes sonication was applied to favor the filling of the porous layer and therefore the formation of a continuous layer. Next, the samples were hung at 90 degrees overnight to remove excess of lubricant.

Roughness characterization: Optical profilometry was used to study surface morphology and to determinate the surface roughness parameters by using a Zeta Instrument profilometer model Z-20 (KLA Company, California, USA). The roughness parameters given in this work were mean values determined from images of each sample at 50x magnification with a field of view of 265 μm × 199 μm recorded. Optical profilometry was also used to monitor the infused layer after the infusion of the lubricant.

Contact and sliding angle: Wettability properties were studied by measuring the contact angle and sliding angle of different liquids on the samples. Water and hexadecane contact angle measurements were obtained using a Attension Theta optical tensiometer (Biolin Scientific, Gothenburg, Sweden) and drop shape analysis. Blood contact angle mesurements were obtained by drop shape analyzer (Kruss DSA30S, Matthews, North Carolina). Contact angles were calculated from the captured images by the Young−Laplace method. Reported contact angles values were the average of at least three 5 μL droplets in different regions. Liquid contact hysteresis was estimated as the minimum tilt angle needed a 5-μL water droplet to roll down the surface. Standard deviations are included.

Turbulence assay: Turbulence experiments have been performed to study the stability of the lubricant layer of the LIS under flow conditions. This is performed by immersion of the LIS in a 500 mL-beaker of distilled water. Turbulence has been obtained by agitation using a magnetic stirrer at 400 rpm. The samples were removed from agitation at different days, left to dry and studied by optical profilometry. The average surface roughness and ratio parameters were obtained to monitor the loss of lubricant on the surface.

Thrombin Generation assay: A fluorogenic thrombin generation assay was performed to study the antithrombogenicity of the different surfaces. Surfaces were cut to 6 mm circles using a biopsy punch and glued to the bottom of a black 96 well-plate (Evergreen Scientific, Vernon, CA, USA) using Elkem Silbione adhesive glue (Factor II, Lakeside, AZ). A fluorogenic solution containing 20 mM Z-Gly-Gly-Arg-AMC (zGGR), 20 mM HEPES buffer (pH 7.4), and 25 mM of $CaCl_2$ was prepared to monitor the clotting formation. 80 μL of citred plasma and 20 μL of 20 mM HEPES buffer were added to the wells. Plates were then incubated at 37°C for 10-15 minutes. After incubation, 100 μL of fluorogenic solution was added to each well and the plate was immediately loaded into the SPECTRAmax fluorescence plate reader (Molecular Devices) to monitor substrate

hydrolysis at 1-minute intervals for 90 minutes. The excitation and emission wavelength were 360 nm and 460nm, respectively. Data collected was analyzed using the Technoclone software – Technothrombin TGA protocol (Vienna, Austria). Lag time to thrombin generation (min), peak thrombin concentration (nM), time to peak thrombin concentration (min) and area under the curve or endogenous thrombin potential (ETP) ($nM \cdot min^{-1}$) were calculated.

Blood adhesion assay: Surfaces were cut to 1x1 cm squares and attached with double-sided tape to the bottom of a 24-well plate. The samples were incubated with 800 µL of citrated whole blood for 20 minutes. Surfaces were removed carefully from the well and the untreated side was cleaned. Then the surfaces were placed in new 24-well plate with 700 µL of DI water. Surfaces were shaken in DI water for 30 minutes at 100 rpm using a shaker (VWR Incubating Mini Shaker, Troemmer, LLC, Thoroface, NJ) to remove adhered blood. 200 µL of the washing solution was placed in a 96-well plate. Absorbance values were measured at 450 nm using plate reader (Synergy Neo2, BioTek, Winooski, Vermont, USA).

Whole blood clotting assay: Surfaces were cut to roughly 0.5 x 1 cm dimensions, weighed using a precision scale (**), then attached to the bottom of a 24-well plate using double-sided tape. 500 µL of citrated whole blood was added to each well, followed by 500 µL of 25mM $CaCl_2$ diluted in 1 M HEPES. Surfaces were incubated for one hour to allow for clot formation. Following incubation surfaces were carefully removed from wells, the untreated side was cleaned, then surfaces were gently washed twice using PBS. Surfaces with adhered blood clots were weighed to then calculate a percent difference in sample mass. Following measurements, surfaces were fixed with 4% formaldehyde for two hours prior to preparation for SEM.

Bacterial adhesion: Samples were cut in 1x2 cm rectangles to form tubes. The tubes were placed in a 96 well-plate. Biofilms of MRSA MW2 were grown on the inner surface of the tubes by diluting overnight culture 1:500 in TSB media enriched with 0.2% sodium citrate, 0.6% yeast extract, and 0.5% glucose (TSBC5) for a total volume of 200 µL/well and incubating for 72 h at 37°C under 180 rpm agitation. After incubation, bacteria were removed and 250 µL of PBS was added to each well to washed it. Samples were then removed from de well plate and washed by immersion in PBS for three times. Then the tubes were placed in 2 mL of Phosphate buffered saline – pH 7.2 (PBS) in an eppendorf tube and vortexed for 2 minutes. The PBS resulting from the washed was serially diluted (1:9 v/v solution with PBS) and plated on tryptic soy agar (TSA) plates. The plated were incubated at 37 °C for 24 hours, and then a colony former unit was performed.

Scanning Electron Microscopy: To evaluate topography and lubricant infusion, surface morphology was imaged by Scanning Electron Microscopy (SEM) using a XL30 microscope

(Philips, Amsterdam, The Netherlands). Samples were coated with a layer of gold-palladium alloy prior to imaging by using a Sputter coater Polaron SC7640.

For the blood adhesion imaging, blood clotting assays surfaces were fixed by performing osmium staining, sequential dehydration using a series of incubations in solutions of increasing concentration of ethanol, then finally critical point drying using the Leica EM CPD300 (Leica Mikrosysteme GmbH, Wien, Austria). Surfaces were mounted on stubs using double-sided carbon tape then coated with approximately 20 nm of gold using a Polaron Model E5100 sputter coater (Polaron Equipment Ltd., Watford, Hertfordshire). Samples were imaged from a top-down perspective using a Tescan Vega II LSU scanning electron microscope (Tescan USA, PA) operating at 10 or 20 kV.

For the bacteria adhesion imaging, planar, A-S, D-S, A-LIS, D-LIS were cut in 1×1 cm size and incubated with MRSA MW2 for 3 days. The bacteria suspension was removed at the end of incubation and the samples were gently washed twice with PBS and fixed with 4% methanol-free formaldehyde for one hour. Fixed samples were dehydrated by submerging in 10, 30, 50, 70, 90, and 100% ethanol solutions for 10 minutes, followed by critical point drying using the Leica EM CPD300 device (Leica Mikrosysteme GmbH, Wien, Austria). Dried samples were mounted with double sided carbon tape on SEM stabs and coated with gold for 2 minutes using a Polaron Model E5100 sputter coater (Polaron Equipment Ltd., Watford, Hertfordshire). SEM imaging was conducted from a top-down perspective using a Tescan Vega II LSU scanning electron microscope (Tescan USA, PA) operating at 10 or 20 kV.

ACKNOWLEDGEMENTS

ABREVIATIONS

LIS – Liquid-infused surface

S-C – Swelling-Coagulation

PVDF – Polyvinylidene fluoride

PTFE – Polytetrafluoroethylene

PMMA – Polymethyl methacrylate

PFD – Perfluorodecaline

PTFS – Poly(3,3,3 - trifluoropropylmethylsiloxane)

REFERENCES

(1)   Jaffer, I. H.; Fredenburgh, J. C.; Hirsh, J.; Weitz, J. I. Medical Device-Induced Thrombosis: What Causes It and How Can We Prevent It? *J. Thromb. Haemost.* **2015**, *13* (S1), S72–S81. https://doi.org/10.1111/jth.12961.

(2)   Badv, M.; Bayat, F.; Weitz, J. I.; Didar, T. F. Single and Multi-Functional Coating Strategies for Enhancing the Biocompatibility and Tissue Integration of Blood-Contacting Medical Implants. *Biomaterials* **2020**, *258* (June), 120291. https://doi.org/10.1016/j.biomaterials.2020.120291.

(3)   Francolini, I.; Donelli, G. Prevention and Control of Biofilm-Based Medical-Device-Related Infections. *FEMS Immunol. Med. Microbiol.* **2010**, *59* (3), 227–238. https://doi.org/10.1111/j.1574-695X.2010.00665.x.

(4)   Badv, M.; Alonso-Cantu, C.; Shakeri, A.; Hosseinidoust, Z.; Weitz, J. I.; Didar, T. F. Biofunctional Lubricant-Infused Vascular Grafts Functionalized with Silanized Bio-Inks Suppress Thrombin Generation and Promote Endothelialization. *ACS Biomater. Sci. Eng.* **2019**, *5* (12), 6485–6496. https://doi.org/10.1021/acsbiomaterials.9b01062.

(5)   Villegas, M.; Zhang, Y.; Badv, M.; Alonso-Cantu, C.; Wilson, D.; Hosseinidoust, Z.; Didar, T. F. Enhancing Osseointegration and Mitigating Bacterial Biofilms on Medical-Grade Titanium with Chitosan-Conjugated Liquid-Infused Coatings. *Sci. Rep.* **2022**, *12* (1), 1–11. https://doi.org/10.1038/s41598-022-09378-4.

(6)   Howell, C.; Grinthal, A.; Sunny, S.; Aizenberg, M.; Aizenberg, J. Designing Liquid-Infused Surfaces for Medical Applications: A Review. *Adv. Mater.* **2018**, *30* (50), 1–26. https://doi.org/10.1002/adma.201802724.

(7)   Bandyopadhyay, S.; Jones, A.; McLean, A.; Sterner, M.; Robbins, C.; Cunningham, M.; Walters, M.; Doddapaneni, K.; Keitel, I.; Gallagher, C. Slippery Liquid Infused Fluoropolymer Coating for Central Lines to Reduce Catheter Associated Clotting and Infections. *Sci. Rep.* **2020**, *10* (1), 1–11. https://doi.org/10.1038/s41598-020-71711-6.

(8)   Khan, S.; Jarad, N. A.; Ladouceur, L.; Rachwalski, K.; Bot, V.; Shakeri, A.; Maclachlan, R.; Sakib, S.; Weitz, J. I.; Brown, E. D.; Soleymani, L.; Didar, T. F. Transparent and Highly Flexible Hierarchically Structured Polydimethylsiloxane Surfaces Suppress

Bacterial Attachment and Thrombosis Under Static and Dynamic Conditions. *Small* **2022**, *2108112*, 2108112. https://doi.org/10.1002/smll.202108112.

(9)   Ladouceur, L.; Shakeri, A.; Khan, S.; Rincon, A. R.; Kasapgil, E.; Weitz, J. I.; Soleymani, L.; Didar, T. F. Producing Fluorine- and Lubricant-Free Flexible Pathogen- and Blood-Repellent Surfaces Using Polysiloxane-Based Hierarchical Structures. *ACS Appl. Mater. Interfaces* **2022**, *14* (3), 3864–3874. https://doi.org/10.1021/acsami.1c21672.

(10)   Kasapgil, E.; Badv, M.; Cantú, C. A.; Rahmani, S.; Erbil, H. Y.; Anac Sakir, I.; Weitz, J. I.; Hosseini-Doust, Z.; Didar, T. F. Polysiloxane Nanofilaments Infused with Silicone Oil Prevent Bacterial Adhesion and Suppress Thrombosis on Intranasal Splints. *ACS Biomater. Sci. Eng.* **2021**, *7* (2), 541–552. https://doi.org/10.1021/acsbiomaterials.0c01487.

(11)   Villegas, M.; Alonso-Cantu, C.; Rahmani, S.; Wilson, D.; Hosseinidoust, Z.; Didar, T. F. Antibiotic-Impregnated Liquid-Infused Coatings Suppress the Formation of Methicillin-Resistant Staphylococcus Aureus Biofilms. *ACS Appl. Mater. Interfaces* **2021**, *13* (24), 27774–27783. https://doi.org/10.1021/acsami.0c19355.

(12)   Wong, T. S.; Kang, S. H.; Tang, S. K. Y.; Smythe, E. J.; Hatton, B. D.; Grinthal, A.; Aizenberg, J. Bioinspired Self-Repairing Slippery Surfaces with Pressure-Stable Omniphobicity. *Nature* **2011**, *477* (7365), 443–447. https://doi.org/10.1038/nature10447.

(13)   Villegas, M.; Zhang, Y.; Abu Jarad, N.; Soleymani, L.; Didar, T. F. Liquid-Infused Surfaces: A Review of Theory, Design, and Applications. *ACS Nano* **2019**, *13* (8), 8517–8536. https://doi.org/10.1021/acsnano.9b04129.

(14)   Guo, Z.; Gao, C.; Li, J.; Liu, Y.; Zheng, Y. Antiicing Properties of Bioinspired Liquid-Infused Double-Layer Surface with Internal Wetting Transport Ability. *Adv. Mater. Interfaces* **2019**, *6* (10), 1–7. https://doi.org/10.1002/admi.201900244.

(15)   Li, J.; Ueda, E.; Paulssen, D.; Levkin, P. A. Slippery Lubricant-Infused Surfaces: Properties and Emerging Applications. *Adv. Funct. Mater.* **2019**, *29* (4), 1–13. https://doi.org/10.1002/adfm.201802317.

(16)   Peppou-Chapman, S.; Hong, J. K.; Waterhouse, A.; Neto, C. Life and Death of Liquid-Infused Surfaces: A Review on the Choice, Analysis and Fate of the Infused Liquid Layer. *Chem. Soc. Rev.* **2020**, *49* (11), 3688–3715. https://doi.org/10.1039/d0cs00036a.

(17)   Yousefi, H.; Samani, S. E.; Khan, S.; Prasad, A.; Shakeri, A.; Li, Y.; Filipe, C. D. M.; Didar, T. F. LISzyme Biosensors: DNAzymes Embedded in an Anti-Biofouling Platform

for Hands-Free Real-Time Detection of Bacterial Contamination in Milk. *ACS Nano* **2022**, *16* (1), 29–37. https://doi.org/10.1021/acsnano.1c05766.

(18)   Shakeri, A.; Jarad, N. A.; Terryberry, J.; Khan, S.; Leung, A.; Chen, S.; Didar, T. F. Antibody Micropatterned Lubricant-Infused Biosensors Enable Sub-Picogram Immunofluorescence Detection of Interleukin 6 in Human Whole Plasma. *Small* **2020**, *16* (45). https://doi.org/10.1002/smll.202003844.

(19)   Khan, S.; Burciu, B.; Filipe, C. D. M.; Li, Y.; Dellinger, K.; Didar, T. F. DNAzyme-Based Biosensors: Immobilization Strategies, Applications, and Future Prospective. *ACS Nano* **2021**, *15* (9), 13943–13969. https://doi.org/10.1021/acsnano.1c04327.

(20)   Smith, J. D.; Dhiman, R.; Anand, S.; Reza-Garduno, E.; Cohen, R. E.; McKinley, G. H.; Varanasi, K. K. Droplet Mobility on Lubricant-Impregnated Surfaces. *Soft Matter* **2013**, *9* (6), 1772–1780. https://doi.org/10.1039/c2sm27032c.

(21)   Kreder, M. J.; Daniel, D.; Tetreault, A.; Cao, Z.; Lemaire, B.; Timonen, J. V. I.; Aizenberg, J. Film Dynamics and Lubricant Depletion by Droplets Moving on Lubricated Surfaces. *Phys. Rev. X* **2018**, *8* (3), 31053. https://doi.org/10.1103/PhysRevX.8.031053.

(22)   Baumli, P.; D'Acunzi, M.; Hegner, K. I.; Naga, A.; Wong, W. S. Y.; Butt, H. J.; Vollmer, D. The Challenge of Lubricant-Replenishment on Lubricant-Impregnated Surfaces. *Adv. Colloid Interface Sci.* **2021**, *287*. https://doi.org/10.1016/j.cis.2020.102329.

(23)   Daniel, D.; Timonen, J. V. I.; Li, R.; Velling, S. J.; Aizenberg, J. Oleoplaning Droplets on Lubricated Surfaces. *Nat. Phys.* **2017**, *13* (10), 1020–1025. https://doi.org/10.1038/nphys4177.

(24)   Agarwal, H.; Breining, W. M.; Lynn, D. M. Continuous Fabrication of Slippery Liquid-Infused Coatings on Rolls of Flexible Materials. *ACS Appl. Polym. Mater.* **2022**, *4* (2), 787–795. https://doi.org/10.1021/acsapm.1c01014.

(25)   Afonso, E.; Martínez-Gómez, A.; Tiemblo, P.; García, N. Industrially Viable Method for Producing All-Polymer Hydrophobic Surfaces Apt for Slippery Liquid-Infused Substrates. *Appl. Surf. Sci.* **2021**, *535* (June 2020), 147728. https://doi.org/10.1016/j.apsusc.2020.147728.

(26)   Saxena, P.; Shukla, P. A Comprehensive Review on Fundamental Properties and Applications of Poly(Vinylidene Fluoride) (PVDF). *Adv. Compos. Hybrid Mater.* **2021**, *4* (1), 8–26. https://doi.org/10.1007/s42114-021-00217-0.

(27) Cardoso, V. F.; Correia, D. M.; Ribeiro, C.; Fernandes, M. M.; Lanceros-Méndez, S. Fluorinated Polymers as Smart Materials for Advanced Biomedical Applications. *Polymers (Basel).* **2018**, *10* (2), 1–26. https://doi.org/10.3390/polym10020161.

(28) Young, T. H.; Lu, J. N.; Lin, D. J.; Chang, C. L.; Chang, H. H.; Cheng, L. P. Immobilization of L-Lysine on Dense and Porous Poly(Vinylidene Fluoride) Surfaces for Neuron Culture. *Desalination* **2008**, *234* (1–3), 134–143. https://doi.org/10.1016/j.desal.2007.09.079.

(29) Abednejad, A.; Ghaee, A.; Morais, E. S.; Sharma, M.; Neves, B. M.; Freire, M. G.; Nourmohammadi, J.; Mehrizi, A. A. Polyvinylidene Fluoride–Hyaluronic Acid Wound Dressing Comprised of Ionic Liquids for Controlled Drug Delivery and Dual Therapeutic Behavior. *Acta Biomater.* **2019**, *100*, 142–157. https://doi.org/10.1016/j.actbio.2019.10.007.

(30) Samree, K.; Srithai, P. U.; Kotchaplai, P.; Thuptimdang, P.; Painmanakul, P.; Hunsom, M.; Sairiam, S. Enhancing the Antibacterial Properties of PVDF Membrane by Hydrophilic Surface Modification Using Titanium Dioxide and Silver Nanoparticles. *Membranes (Basel).* **2020**, *10* (10), 1–18. https://doi.org/10.3390/membranes10100289.

(31) Niizeki, K.; Nishidate, I.; Uchida, K.; Kuwahara, M. Unconstrained Cardiorespiratory and Body Movement Monitoring System for Home Care. *Med. Biol. Eng. Comput.* **2005**, *43* (6), 716–724. https://doi.org/10.1007/BF02430948.

(32) Lei, K. F.; Hsieh, Y. Z.; Chiu, Y. Y.; Wu, M. H. The Structure Design of Piezoelectric Poly(Vinylidene Fluoride) (PVDF) Polymer-Based Sensor Patch for the Respiration Monitoring under Dynamic Walking Conditions. *Sensors (Switzerland)* **2015**, *15* (8), 18801–18812. https://doi.org/10.3390/s150818801.

(33) Sharma, T.; Aroom, K.; Naik, S.; Gill, B.; Zhang, J. X. J. Flexible Thin-Film PVDF-TrFE Based Pressure Sensor for Smart Catheter Applications. *Ann. Biomed. Eng.* **2013**, *41* (4), 744–751. https://doi.org/10.1007/s10439-012-0708-z.

(34) Sasaki, H.; Kanti Bala, P.; Yoshida, H.; Ito, E. Miscibility of PVDF/PMMA Blends Examined by Crystallization Dynamics. *Polymer (Guildf).* **1995**, *36* (25), 4805–4810. https://doi.org/10.1016/00323-8619(59)92967-.

(35) Zhou, X.; Cakmak, M. Phase Behavior of Rapidly Quenched PVDF/PMMA Blends as Characterized by Raman Spectroscopy, X-Ray Diffraction and Thermal Techniques. *J. Macromol. Sci. Part B Phys.* **2007**, *46 B* (4), 667–682. https://doi.org/10.1080/00222340701388680.

(36)   Song, H.; Yang, S.; Sun, S.; Zhang, H. Effect of Miscibility and Crystallization on the Mechanical Properties and Transparency of PVDF/PMMA Blends. *Polym. - Plast. Technol. Eng.* **2013**, *52* (3), 221–227. https://doi.org/10.1080/03602559.2012.735314.

(37)   Ruan, L.; Yao, X.; Chang, Y.; Zhou, L.; Qin, G.; Zhang, X. Properties and Applications of the β Phase Poly(Vinylidene Fluoride). *Polymers (Basel).* **2018**, *10* (3), 1–27. https://doi.org/10.3390/polym10030228.

(38)   Mackie, G.; Gao, L.; Yau, S.; Leslie, D. C.; Waterhouse, A. Clinical Potential of Immobilized Liquid Interfaces: Perspectives on Biological Interactions. *Trends Biotechnol.* **2019**, *37* (3), 268–280. https://doi.org/10.1016/j.tibtech.2018.08.003.

(39)   Yang, Z.; Bai, Y.; Meng, L.; Wang, Y.; Pang, A.; Guo, X.; Xiao, J.; Li, W. A Review of Poly[(3,3,3-Trifluoropropyl)Methylsiloxane]: Synthesis, Properties and Applications. *Eur. Polym. J.* **2022**, *163* (July 2021), 110903. https://doi.org/10.1016/j.eurpolymj.2021.110903.

(40)   Miyamoto, K.; Refojo, M. F.; Tolentino, F. I.; Fournier, G. A.; Albert, D. M. Fluorinated Oils as Experimental Vitreous Substitutes. *Arch. Ophthalmol.* **1986**, *104* (7), 1053–1056. https://doi.org/10.1001/archopht.1986.01050190111048.

(41)   Gremillion, C. M.; Peyman, G. A.; Liu, K. R.; Naguib, K. S. Fluorosilicone Oil in the Treatment of Retinal Detachment. *Br. J. Ophthalmol.* **1990**, *74* (11), 643–646. https://doi.org/10.1136/bjo.74.11.643.

(42)   Afonso, E.; Martínez-Gómez, A.; Tiemblo, P.; García, N. Industrially Viable Method for Producing All-Polymer Hydrophobic Surfaces Apt for Slippery Liquid-Infused Substrates. *Appl. Surf. Sci.* **2021**, *535* (August 2020), 147728. https://doi.org/10.1016/j.apsusc.2020.147728.

(43)   Tanaka, A.; Kojima, Y. Application of Poly(Vinylidene Fluoride) and Poly(Methyl Methacrylate) Blends to Optical Discs. *Kobunshi Ronbunshu* **1990**, *47* (12), 989–991. https://doi.org/10.1295/koron.47.989.

(44)   Zhu, H.; Dai, Z.; Tu, W. Study on the Preparation and Performance of Low Gas Permeability Trifluoropropyl Phenyl Silicone Rubber. *RSC Adv.* **2017**, *7* (63), 39739–39747. https://doi.org/10.1039/c7ra07195g.

(45)   Vargaftik, N. B.; Volkov, B. N.; Voljak, L. D. International Tables of Water Surface Tension. *J. Phys. Chem. Ref. Data* **1983**, *12* (3), 817–820.

(46)   Hrnčíř, E.; Rosina, J. Surface Tension of Blood. *Physiol. Res.* **1997**, *46* (4), 319–321.

(47) McHale, G.; Orme, B. V.; Wells, G. G.; Ledesma-Aguilar, R. Apparent Contact Angles on Lubricant-Impregnated Surfaces/SLIPS: From Superhydrophobicity to Electrowetting. *Langmuir* **2019**, *35* (11), 4197–4204. https://doi.org/10.1021/acs.langmuir.8b04136.

(48) Turner, N. A.; Sharma-Kuinkel, B. K.; Maskarinec, S. A.; Eichenberger, E. M.; Shah, P. P.; Carugati, M.; Holland, T. L.; Fowler, V. G. Methicillin-Resistant Staphylococcus Aureus: An Overview of Basic and Clinical Research. *Nat. Rev. Microbiol.* **2019**, *17* (4), 203–218. https://doi.org/10.1038/s41579-018-0147-4.

(49) Yau, J. W.; Stafford, A. R.; Liao, P.; Fredenburgh, J. C.; Roberts, R.; Weitz, J. I. Mechanism of Catheter Thrombosis: Comparison of the Antithrombotic Activities of Fondaparinux, Enoxaparin, and Heparin in Vitro and in Vivo. *Blood* **2011**, *118* (25), 6667–6674. https://doi.org/10.1182/blood-2011-07-364141.

ToC